Journal of Zhejiang University-SCIENCE A (Applied Physics & Engineering)
ISSN 1673-565X (Print); ISSN 1862-1775 (Online)
www.jzus.zju.edu.cn; www.springerlink.com
E-mail: jzus@zju.edu.cn

A parametric sensitivity study by numerical simulations on plume dispersion of the exhaust from a cryogenic wind tunnel*

Jing-feng LI[1], Kai WANG[1,2], Xiao-bin ZHANG[1], Xia ZHOU[1], Li-min QIU[†‡1]

[1]*Institute of Refrigeration and Cryogenics, Zhejiang University, Hangzhou 310027, China*

[2]*Department of Chemical Engineering, Imperial College London, London SW7 2AZ, UK*

[†]E-mail: Limin.Qiu@zju.edu.cn

Received Nov. 26, 2017; Revision accepted Mar. 29, 2018; Crosschecked Sept. 12, 2018

Abstract: The low temperature plume exhausted from a cryogenic wind tunnel may sink down, posing a severe threat to public health and safety. Quantitative risk assessment of cryogenic plume flow behavior therefore plays an important role in the design and optimization of a cryogenic wind tunnel. A numerical model with a modified Hertz-Knudsen relation considering the phase change physics of the small quantity of water involved is applied to analyze the dispersion of the low temperature nitrogen plume exhausted from a 0.3 m cryogenic wind tunnel. The homogeneous multiphase flow is modeled using the single-fluid mixture model. A model validation is presented for the exhaust plume from the US National Transonic Facility (NTF). The predicted results are found to be better than those predicted by National Aeronautics and Space Administration (NASA)'s two-stage analytical model. The influences of the environmental wind speed, the environmental wind temperature, the relative humidity, and the exhaust flow rate, on low temperature nitrogen plume dispersion are obtained. In particular, the parametric sensitivities of different influence factors are analyzed. The environmental wind temperature and the exhaust flow rate of the nitrogen gas have greater impact on the temperature of the plume near the ground than do the environmental wind speed and the relative humidity. The exhaust flow rate of the nitrogen gas has greater impact on the oxygen concentration near the ground than does the environmental wind speed, while the environmental wind temperature and the relative humidity have negligible impacts. The results provide guidance on the operation and design improvement of a cryogenic gaseous nitrogen discharge system to avoid its potential hazards.

Key words: Cryogenic wind tunnel; Plume dispersion; Computational fluid dynamics (CFD); Phase change
https://doi.org/10.1631/jzus.A1700632 **CLC number:** TQ021.4

1 Introduction

A cryogenic wind tunnel is essential for the high Reynolds number and low energy-consumption tests in the research and development of large aircraft (Kilgore, 1994, 2005). Based on a theoretical investigation by Smelt (1945), the US National Transonic Facility (NTF) combines a modern wind tunnel with a large-scale cryogenic engineering system which can inject liquid nitrogen at rates up to 450 kg/s to maintain the required low temperature test environment (Kilgore, 2005). This leads to a large quantity of nitrogen gas being discharged into the environment. While a cryogenic wind tunnel is running, a large amount of low temperature nitrogen gas, denser than the ambient air, may sink down (Ivey, 1979), posing potential hazards to the public such as frostbite damage and oxygen deficiency. Therefore, the quantitative risk of the cryogenic plume flow behavior for a cryogenic wind tunnel cannot be ignored and should be assessed.

‡ Corresponding author

* Project supported by the National Key R&D Program of China (No. 2017YFB0603701), the Key Program of the National Natural Science Foundation of China (No. 51636007), and partly supported by the China Aerodynamics Research and Development Center

ORCID: Jing-feng LI, https://orcid.org/0000-0002-5780-3192; Li-min QIU, https://orcid.org/0000-0003-1943-8902

There is much experimental research on conventional dense gases (natural gas, ammonia gas, chlorine gas etc.). Liquid natural gas (LNG) spill tests, the Burro series (Koopman et al., 1982), and the Coyote series (Goldwire et al., 1983), were carried out by Lawrence Livermore National Laboratory supported by the US Department of Energy, and the concentration and temperature changes during dispersion in different emission conditions were recorded. Different from the Burro series and the Coyote series in the open environment with flat terrain, the Falcon series (Brown et al., 1990) focused on the impacts of buildings and walls on natural gas dispersion after LNG spilling in a square pond with walls and a barrier. Another strategy is the wind tunnel test with a scaled model, for example, chlorine gas dispersion in complex terrain (McBride et al., 2001) and LNG leaking from a tank (Ohba et al., 2004). For all the experimental methods mentioned above, specific equipment is necessary, and the pre-preparation, as well as the operation itself, requires a lot of manpower and time. Likewise, the design and operation of an experiment on the plume dispersion of a specific cryogenic tunnel involve a huge cost of resources, time, and labor.

Compared to the experimental study, a simulation study based on computational fluid dynamics (CFD) can be a good alternative for risk analysis because of its high efficiency and low cost. In recent years, CFD has become the favoured method for the study of cryogenic gas dispersion. CFD codes based on the Navier-Stokes equations for species, mass, momentum, and energy conservation, have the ability to solve 3D plume problems taking into account turbulent mixing, variable fluid physical properties, complex terrain and obstacles in the path of a dispersing fluid (McBride et al., 2001; Sklavounos and Rigas, 2006; Luketa-Hanlin et al., 2007; Tauseef et al., 2011). To avoid the potential hazards of a cryogenic plume, National Aeronautics and Space Administration (NASA) focused on research into the gaseous nitrogen vent system (Kilgore, 1976; Ivey, 1979; Bruce et al., 1984) and developed a two-stage analytical model (Lassiter, 1987) to simulate the process of cryogenic plume dispersion. However, the agreement between the simulation by the two-stage analytical model and the experimental data needs to be improved. In our previous work, a numerical model considering the phase change physics of the small quantity of water involved was developed, leading to calculations more consistent with experiments than those ignoring the phase change (Zhang et al., 2015). It is far from enough just to predict the cryogenic plume flow behavior in some certain conditions. The influences of some important parameters on the plume dispersion of the exhaust from a cryogenic wind tunnel also need to be analyzed.

As shown in Fig. 1, the low temperature environment in the 0.3 m cryogenic wind tunnel is achieved by injecting liquid nitrogen through small nozzles positioned in the wind tunnel circuit upstream of the driven fan. Then the liquid sprayed into the tunnel is vaporized and the cold nitrogen gas is accelerated as the test gas. On the other hand, in order to keep steady thermodynamic conditions for testing, it is necessary to exhaust the cold nitrogen gas from the tunnel through an exhaust stack, at the same mass flow rate as that of the liquid nitrogen which is continuously injected.

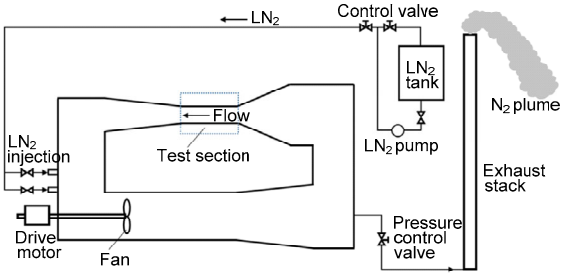

Fig. 1 Sketch of the 0.3-m cryogenic wind tunnel

In this study, the model developed by considering the phase change (Zhang et al., 2015) is applied to simulate the dispersion of the low temperature nitrogen gas exhausted from a 0.3-m cryogenic wind tunnel. Solutions are obtained based on the single-fluid homogenous mixture model. The experiment of the plume exhausting from the US NTF is modeled, and the developed model is validated as more accurate than the two-stage analytical model. The purpose of this study is to quantitatively analyze the parametric effects, including the environmental wind speed, the environmental wind temperature, the relative humidity, and the exhaust flow rate, on the pure nitrogen plume (at 110 K) dispersion of the 0.3-m cryogenic wind tunnel.

2 Mathematical model

The discharge and dispersion of the low temperature nitrogen plume are modeled using the 3D, transient, compressible conservation equations governing two-phase flows.

The continuity, momentum, and energy equations are given below:

$$\frac{\partial}{\partial t}\left(\rho_{\mathrm{m}}\right)+\nabla\cdot\left(\rho_{\mathrm{m}}\overline{u}_{\mathrm{m}}\right)=0, \tag{1}$$

$$\begin{aligned}&\frac{\partial}{\partial t}\left(\rho_{\mathrm{m}}\overline{u}_{\mathrm{m}}\right)+\nabla\cdot\left(\rho_{\mathrm{m}}\overline{u}_{\mathrm{m}}\overline{u}_{\mathrm{m}}\right)\\&\quad=\nabla\cdot\left[\mu_{\mathrm{m}}\left(\nabla\overline{u}_{\mathrm{m}}+\nabla\overline{u}_{\mathrm{m}}^{\mathrm{t}}\right)\right]+\rho_{\mathrm{m}}g\\&\qquad+\nabla\cdot\left[\sum_{k=1}^{2}\left(\alpha_k\rho_k\overline{u}_{\mathrm{dr},k}\overline{u}_{\mathrm{dr},k}\right)\right]-\nabla p,\end{aligned} \tag{2}$$

$$\begin{aligned}&\frac{\partial}{\partial t}\sum_{k=1}^{2}\left(\alpha_k\rho_kE_k\right)+\nabla\cdot\sum_{k=1}^{2}\left[\alpha_k\overline{u}_k\left(\alpha_kE_k+p\right)\right]\\&\quad=\nabla\cdot\left(k_{\mathrm{eff}}\nabla T\right)+S_{\mathrm{E}},\end{aligned} \tag{3}$$

where t is the time, ρ is the density, $\overline{u}$ is the mean velocity, μ is the viscosity, g is the gravitational acceleration, α is the volume fraction, p is the pressure, E is the energy, and T is the temperature. The superscript t indicates turbulence, the subscript k denotes liquid phase or gas phase, and the subscript m represents phase mixture. S_{E} includes the volumetric heat source due to the phase change. In our case, energy E_k equals the enthalpy h_k. The effective thermal conductivity is $k_{\mathrm{eff}}=\sum_{k=1}^{2}\left[\alpha_k\left(k_k+k_k^{\mathrm{t}}\right)\right]$. For the mixture, $\rho_{\mathrm{m}}=\sum_{k=1}^{2}(\alpha_k\rho_k)$, $\overline{u}_{\mathrm{m}}=\frac{\sum_{k=1}^{2}(\alpha_k\rho_k\overline{u}_k)}{\rho_{\mathrm{m}}}$, and $\mu_{\mathrm{m}}=\sum_{k=1}^{2}(\alpha_k\mu_k)$. $\overline{u}_{\mathrm{dr},k}$ is the drift velocity for phase k, $\overline{u}_{\mathrm{dr},k}=\overline{u}_k-\overline{u}_{\mathrm{m}}$.

The realizable κ-ε model (McBride et al., 2001) used in our simulations is presented as follows in the mixture model:

$$\begin{aligned}&\frac{\partial}{\partial t}\left(\rho_{\mathrm{m}}\kappa\right)+\frac{\partial}{\partial x_j}\left(\rho_{\mathrm{m}}\overline{u}_{\mathrm{m},j}\kappa\right)\\&\quad=\frac{\partial}{\partial x_j}\left[\left(\mu_{\mathrm{m}}+\frac{\mu_{\mathrm{m}}^{\mathrm{t}}}{\sigma_k}\right)\frac{\partial\kappa}{\partial x_j}\right]+G_\kappa+G_b-\rho_{\mathrm{m}}\varepsilon,\end{aligned} \tag{4}$$

$$\begin{aligned}&\frac{\partial}{\partial t}\left(\rho_{\mathrm{m}}\varepsilon\right)+\frac{\partial}{\partial x_j}\left(\rho_{\mathrm{m}}\overline{u}_{\mathrm{m},j}\varepsilon\right)=\frac{\partial}{\partial x_j}\left[\left(\mu_{\mathrm{m}}+\frac{\mu_{\mathrm{m}}^{\mathrm{t}}}{\sigma_\varepsilon}\right)\frac{\partial\varepsilon}{\partial x_j}\right]\\&\quad+\rho_{\mathrm{m}}C_1S\varepsilon-\rho_{\mathrm{m}}C_2\frac{\varepsilon^2}{\kappa+\sqrt{\nu\varepsilon}}+C_{1\varepsilon}\frac{\varepsilon}{\kappa}C_{3\varepsilon}G_b,\end{aligned} \tag{5}$$

where κ is the turbulence kinetic energy and ε is the dissipation. σ_κ and σ_ε are respectively the inverse effective Prandtl numbers of κ and ε equations. ν is the kinematic viscosity, G_κ represents the generation of turbulence kinetic energy due to the mean velocity gradients, and G_b is the generation of turbulence kinetic energy due to buoyancy. $\eta=S\frac{\kappa}{\varepsilon}$, $S=\sqrt{2S_{i,j}S_{i,j}}$, $S_{i,j}=\frac{1}{2}\left(\frac{\partial u_{\mathrm{m},j}}{\partial x_i}+\frac{\partial u_{\mathrm{m},i}}{\partial x_j}\right)$. C_1, C_2, $C_{1\varepsilon}$, and $C_{3\varepsilon}$ are constants, $C_1=\max\left[0.43,\frac{\eta}{\eta+5}\right]$. The turbulence viscosity $\mu_{\mathrm{m}}^{\mathrm{t}}$ is linked to κ and ε via the relation:

$$\mu_{\mathrm{m}}^{\mathrm{t}}=C_\mu\rho_{\mathrm{m}}\frac{\kappa^2}{\varepsilon}. \tag{6}$$

The definitions of C_μ can be found in (ANSYS, 2011).

From the continuity equation for liquid phase, the volume fraction equation can be obtained:

$$\frac{\partial}{\partial t}(\alpha_{\mathrm{l}}\rho_{\mathrm{l}})+\nabla\cdot\left(\alpha_{\mathrm{l}}\rho_{\mathrm{l}}\overline{u}_{\mathrm{m}}\right)=\dot{m}_{\mathrm{gl}}-\dot{m}_{\mathrm{lg}}, \tag{7}$$

where $\dot{m}_{\mathrm{gl}}$ and $\dot{m}_{\mathrm{lg}}$ are respectively the mass transfer rate from the gas to the liquid phase, and vice versa. The subscript l represents liquid phase, and g represents the gas phase.

The local mass fraction of each species $Y_{\mathrm{g},s}$ in the gas mixture can be solved through the solution of a convection-diffusion equation for the sth species:

$$\begin{aligned}&\frac{\partial}{\partial t}\left(\rho_{\mathrm{g}}\alpha_{\mathrm{g}}Y_{\mathrm{g},s}\right)+\nabla\cdot\left(\rho_{\mathrm{g}}\alpha_{\mathrm{g}}\overline{u}Y_{\mathrm{g},s}\right)\\&\quad=-\nabla\cdot\alpha_{\mathrm{g}}\overline{J}_{\mathrm{g},s}+\dot{m}_{\mathrm{lg},s}-\dot{m}_{\mathrm{gl},s}.\end{aligned} \tag{8}$$

$\bar{J}_{g,s}$, the diffusion flux of species s, has the following form in turbulent flows:

$$\bar{J}_{g,s} = -\left(\rho D_{g,s} + \frac{\mu^t}{Sc^t}\right)\nabla Y_{g,s}, \tag{9}$$

where Sc^t is the effective Schmidt number for the turbulent flow, $Sc^t = \dfrac{\mu^t}{\rho D^t}$, and D^t is the turbulent diffusion coefficient. $D_{g,s}$ is the mass diffusion coefficient due to the molecular diffusion for laminar flow.

The evaporation-condensation flux F based on kinetic theory for a flat interface can be given by the Hertz-Knudsen formula (Marek and Straub, 2001):

$$F = C\sqrt{\frac{M}{2\pi RT}}\left(p_{sat} - p_v\right), \tag{10}$$

where M is the mass per mole, R is the universal gas constant, p_v represents the vapor partial pressure at the interface on the gas side, and p_{sat} is the saturation pressure corresponding to the current temperature T_{sat}. The coefficient C is the vaporization or condensation coefficient.

Using the Clausius–Clapeyron equation to modify the Hertz-Knudsen relation, for a gas mixture with two or more components, the volume mass transfer rate per unit of the species in Eq. (8) is given as follows (Zhang et al., 2015):

$$\begin{cases} \dot{m}_{lg,s} = F\cdot\dfrac{A_s}{V_{cell}} = C_{ev}\cdot\alpha_l\cdot\left[\alpha_l\rho_l\left(\dfrac{T_l - T_{sat}}{T_{sat}}\right)\right], \\ \qquad \text{evaporation } (T_l > T_{sat}); \\ \dot{m}_{gl,s} = F\cdot\dfrac{A_s}{V_{cell}} = C_{con}\cdot\chi_s\cdot\left[\alpha_g\rho_l\left(\dfrac{T_g - T_{sat}}{T_{sat}}\right)\right], \\ \qquad \text{condensation } (T_g < T_{sat}), \end{cases} \tag{11}$$

where χ_s is the molar fraction of condensation species in the gas mixture, A_s is the mass transfer area, and V_{cell} is the cell volume. The condensation coefficient C_{con} is generally higher than the evaporation coefficient C_{ev} (Marek and Straub, 2001), and it is reasonable to assume that C_{con}=1.2C_{ev} (Rubel and Gentry, 1984). Consistent with our previous study (Zhang et al., 2015), the coefficients C_{ev}=100 and C_{con}=120 are used in all the following simulations.

3 Modeling approach

3.1 Problem description and boundary condition

The cold nitrogen gas is discharged from the wind tunnel through a vent stack of 0.75 m in diameter (d=0.75 m) and 13 m in height (h=13 m). The lowest temperature of the exhausted nitrogen gas is 110 K, while the mass flow rate varies from 0.06 kg/s to 5.60 kg/s. As the low temperature nitrogen gas is denser than the ambient air, the plume may sink down and pose a severe threat to public health and safety through the hazards of frostbite and oxygen deficiency. In addition, a water mist will reduce local visibility within the descent of the plume.

Fig. 2 shows the corresponding computation domain for the CFD simulation. The computational domain is large enough to capture the features of the plume dispersion. The dimensions of the model are 80 m×80 m×150 m in the x, y, z directions, respectively. The center of the bottom of the vent stack is set as the origin of the coordinates.

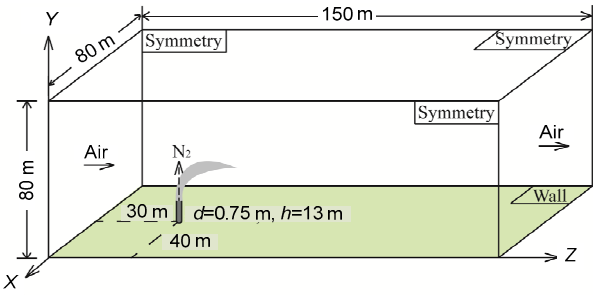

Fig. 2 Computation domain for the CFD simulation

The boundary types of the simulation domain are presented in Table 1. The constant inlet air velocity (Table 2) is applied at the left surface; the constant inlet N_2 velocity (Table 2) with a given temperature of 110 K is specified at the top surface of the exhaust stack; the constant pressure is applied at the right surface; the front and the rear surfaces, as well as the top surface, which presumably are far enough from the plume, are specified as the symmetry condition (Chan et al., 1982); the ground is specified as a heat insulated wall (Ermak et al., 1989; Luketa-Hanlin et al., 2007).

3.2 Grid independency

The time series data simulated with different types of grids, i.e. 2945049 (thin mesh), 5298146

(original mesh), and 6750824 (refined mesh) of two positions at L=2 m (H=10 m above ground) and L=5 m (H=0.5 m above ground) downwind of the tunnel exhaust ejector center are monitored. In this simulation for mesh independence analysis, the nitrogen gas exhaust flow rate is 5.6 kg/s and the exit temperature is 110 K, while the environmental wind speed is 0.4 m/s, the environmental wind temperature is 296 K, and the relative humidity is 50%. The temperature and the oxygen molar concentration at L=2 m (H=10 m) are presented in Fig. 3 and Fig. 4, respectively. Considering the grid independency and the computation efficiency, the mesh with 5298146 cells is adopted in the following simulation.

Table 1 Boundary types of the simulation domain

Boundary name	Boundary type
Air-inlet (left)	Velocity-inlet
N_2-inlet (top of the stack)	Velocity-inlet
Air-outlet (right)	Pressure-outlet
Top	Symmetry
Front/Rear	Symmetry
Ground	Wall

3.3 Solution methods

The pressure-based unsteady calculations for complex species transport in multiphase flows with mass transfer between the phases are solved numerically using Fluent. The pressure implicit split operator (PISO) algorithm is applied to implement the multiphase formulation, solving the governing equations of continuity, momentum, and energy in sequence. The convective terms and the diffusive terms are discretized using the second-order accurate upwind scheme and the second-order accurate central scheme, respectively. The vapor fraction equation, the species transfer equations, and the two turbulent equations are discretized using the first-order upwind scheme. The convergence criteria in the present study are at least a drop of three orders of magnitude in the mass, momentum, and vapor transfer equations, and of six orders in the energy equation, which are deemed sufficient for the present flow solutions.

3.4 Physical properties

It is assumed that the environmental air is a mixture of N_2, O_2, and H_2O. The thermodynamic

Table 2 Primary simulated conditions in different cases

Case	Wind speed (m/s)	Wind temperature (K)	Exhaust gas component (in weight)	Exhaust flow rate (m/s)/ N_2 flow rate (kg/s)	Exhaust temperature (K)	Relative humidity (%)	Initial air components (mole fraction: $N_2/O_2/H_2O$)
Validation	2.68	281.9	N_2:air=1:1.5; N_2:air=1:1.2	42.30/207.70; 49.20/270.70	238 232	94	78.11/20.76/1.13
Section 5.1	1; 3; 6; 9	296	Pure N_2	4.12/5.60	110	50	77.84/20.69/1.47
Section 5.2	1	280; 290; 296; 310	Pure N_2	4.12/5.60	110	50	77.84/20.69/1.47
Section 5.3	1	296	Pure N_2	4.12/5.60	110	10; 30; 50; 70; 90	78.77/20.94/0.29; 78.30/20.81/0.88; 77.84/20.69/1.47; 77.37/20.57/2.06; 76.90/20.44/2.65
Section 5.4	1	296	Pure N_2	0.04/0.06; 0.07/0.10; 0.15/0.20; 0.37/0.50; 0.74/1.00; 1.47/2.00; 2.94/4.00; 4.12/5.60	110	50	77.84/20.69/1.47

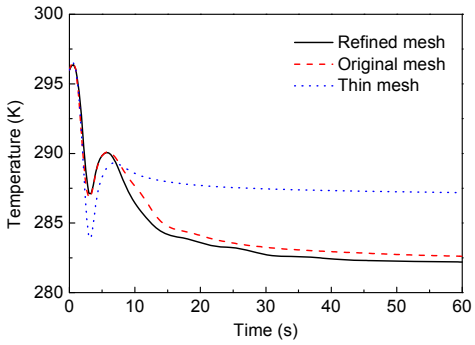

Fig. 3 Simulated temperature time series with different meshes at L=2 m, H=10 m

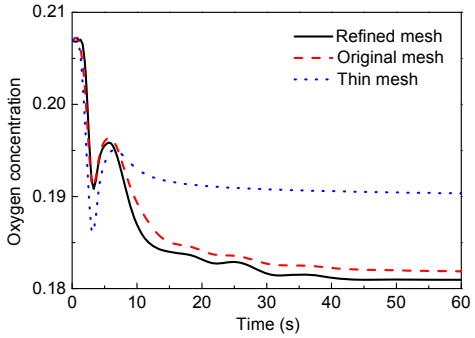

Fig. 4 Simulated oxygen concentration time series with different meshes at L=2 m, H=10 m

properties of all the pure components are acquired from the databank software REFPROP issued by National Institute of Standards and Technology (NIST, 2007). Specifically, the specific heats of all gas species, as well as the viscosities and the thermal conductivities of the oxygen and the nitrogen, are specified as temperature-dependent. All the physical properties of the water vapor or the condensed water are given as constant in view of its small volume fraction in the mixture.

The thermal conductivity, viscosity, and specific heat of the gas mixture are calculated by the mixing law as

$$\varphi = \sum\nolimits_s Y_s \varphi_s, \tag{12}$$

where Y_s is the mass fraction of species s.

4 Model validation

The experimental records of the plume exhausting from the US NTF (Lassiter, 1987) are used for validating the model. Low temperature nitrogen gas was discharged from the top of the vent stack which is 3.35 m in diameter, 36.6 m in height. Lassiter (1987) developed a two-stage analytical model to predict the behavior of the plume exhausting from the US NTF. The first stage of the model was solved based on the Gaussian dispersion model, while the second stage during the descent of the plume was solved by describing the crosswind displacements by vorticity and numerically integrating in the crosswind and downwind directions. Two cases of the plume during tunnel nitrogen exhaust flows of 207.7 kg/s (~238 K) and 270.7 kg/s (~232 K) are simulated using Fluent. For the two cases, the environmental wind temperature is 281.9 K, the environmental wind speed is 2.68 m/s, and the relative humidity is 94%. The simulated results by Fluent are compared with the test results and with the behaviors predicted by Lassiter's model.

To validate the model, two key parameters of the plume's centerline in the experiment and the simulation results by Lassiter's model and by Fluent (the present work) are listed in Table 3. Fig. 5 presents the contour of the liquid water concentration of the cryogenic plume calculated by Fluent for the case with nitrogen flow rate 270.7 kg/s. Fig. 6 presents the contours of the temperature and the oxygen concentration in the same case. It can be seen from Table 3, for the centerline maximum height, that the deviations by Fluent are relatively smaller than those by Lassiter's, while the deviations in Fluent are significantly smaller for the distance downwind of centerline at maximum height in both cases. The comparisons indicate that the numerical model in this work is much more accurate, which is more reliable for risk assessment.

Table 3 Comparisons of simulated centerline parameters with experimental data

Method	Centerline maximum height (m)		Distance downwind of centerline at maximum height (m)	
	a	b	a	b
Experiment	105.9	119.0	59.7	97.3
Lassiter's model	116.7 (+10.2%)	135.0 (+13.4%)	120.5 (+101.8%)	148.8 (+52.9%)
Present model	107.3 (+1.3%)	127.0 (+6.7%)	77.7 (+30.2%)	106.3 (+9.3%)

a: 207.7 kg/s nitrogen flow rate; b: 270.7 kg/s nitrogen flow rate. The relative errors are inside the brackets

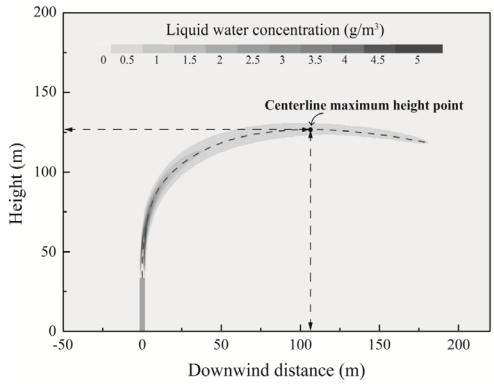

Fig. 5 Contour of the liquid water concentration of the plume calculated by Fluent for the case with a nitrogen flow rate 270.7 kg/s

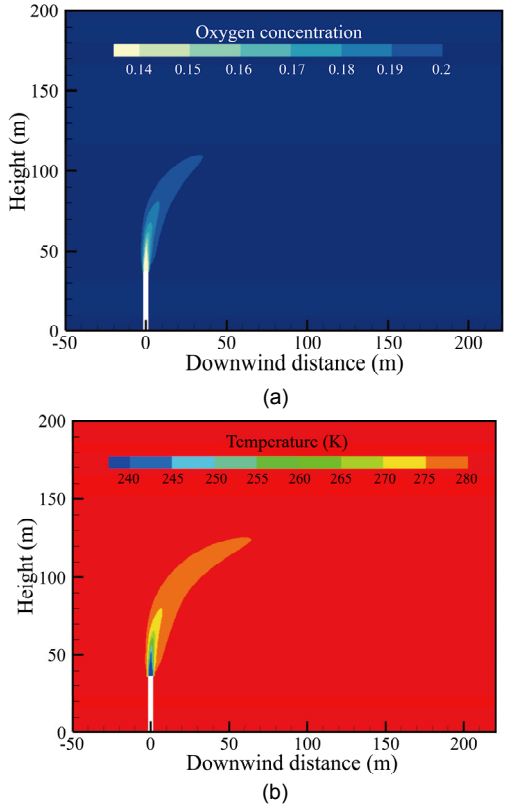

Fig. 6 Contours of the oxygen concentration (a) and the temperature (b)

5 Results and analyses

The dispersion of a cryogenic wind tunnel exhaust plume is a complex physical process of heat and mass transfer. The exhaust nitrogen gas has an upward movement trend due to the initial velocity after jetting from the vent stack. At the same time, the ambient air is entrained in the low temperature nitrogen gas, leading to the formation of a visible water mist. The water vapor in the air is condensed as a result of the intensive turbulent mixing of the cold and the hot gases. The nitrogen component is continuously diluted and the temperature of the cloud gets higher as the cloud spreads downwind at roughly environmental wind speed or less since the hot air is continually mixed in. Eventually, the temperature of the cloud will increase until it is equal to the temperature of the ambient air, and the formed droplets will vaporize.

Many factors affect the low temperature nitrogen plume dispersion. For the cryogenic plume with a certain exhaust temperature (110 K), the most obvious factors include the velocity, the temperature, and the relative humidity of the environmental wind, as well as the flow rate of the exhaust gas; their effects on the cryogenic plume dispersion will be analyzed. This study focuses on the impact of different values of the influence factors on the plume descent, while the horizontal dispersion range is out of its scope.

5.1 Effect of environmental wind speed

The environmental wind is always a key factor in enhancing the local mixing of the plume gas and the ambient air. Cases with different environmental wind speeds (i.e. 1 m/s, 3 m/s, 6 m/s, and 9 m/s) are simulated to investigate the effect of environmental wind speed on the cryogenic plume dispersion. In these cases, the other parameters are consistent: the environmental wind temperature is 296 K; the relative humidity is 50%; the exhaust flow rate of the low temperature (110 K) nitrogen gas is 5.6 kg/s.

The predicted minimal temperatures and minimal oxygen concentrations at H=1.5 m with phase change are always greater than those without phase change (Fig. 7). That is because the water condensation process releases additional heat and the smaller local temperature difference leads to a slower descent due to the smaller local density difference. With increased environmental wind speed, both the minimal temperatures and the minimal oxygen concentrations rise as a result of local mixing enhancement, since the raising environmental wind speed causes more plume gas to be dispersed and propelled forward in the ambient air (Mousavi and Parvini, 2016). When the environmental wind speed reaches 9 m/s, as a

consequence of sufficient mixing, both the minimal temperature and the minimal oxygen concentration at H=1.5 m regardless of modeling the phase change are almost the same as those of the ambient air. The predicted maximum liquid water concentrations in the whole domain and at H=1.5 m under different environmental wind speed conditions are presented in Table 4. Inconsistent with the trends of the minimal temperature and the minimal oxygen concentration, the maximum liquid water concentration at H=1.5 m decreases as the environmental wind speed increases, while the maximum liquid water concentration in the whole domain increases. The possible reason for these outcomes is that the liquid water in the plume has the physical process from generation to dissipation. In the early stage of the plume dispersion, more vapor water is condensed with the local mixing enhancement by raising environmental wind speed. As a result, the maximum liquid water concentration in the whole domain increases. However, the mist dissipation is enhanced as the environmental wind velocity increases, leading to lower maximum liquid water concentration at H=1.5 m after the descent process.

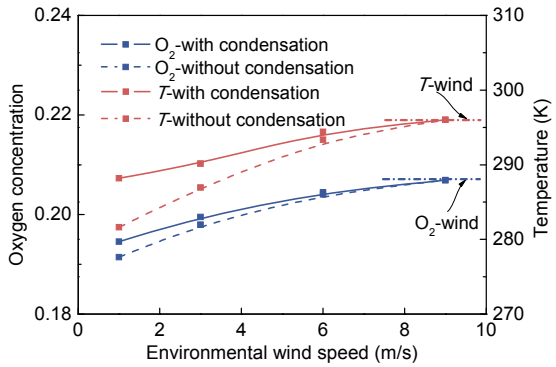

Fig. 7 Simulated minimal oxygen concentrations and minimal temperatures at H=1.5 m with different environmental wind speeds

Table 4 Simulated results of water concentration with different environmental wind speeds

Environmental wind speed (m/s)	Max liquid water concentration in the whole domain (g/m^3)	Max liquid water concentration at H=1.5 m (g/m^3)
1	10.42	2.44
3	11.17	1.98
6	12.84	0.36
9	14.99	0

According to the simulated minimal oxygen concentrations and minimal temperatures near the ground, the sink down phenomenon is more significant with the environmental wind speed 1 m/s than the others. The typical environmental wind speed on the site is 1 m/s. Thus, in the study of the other parameters, 1 m/s is chosen as the standard environmental wind speed to guarantee sufficiently variable ranges of the minimal oxygen concentrations and the minimal temperatures near the ground.

5.2 Effect of environmental wind temperature

The environmental wind temperature significantly affects the heat exchange between the plume gas and the ambient air. Cases with different environmental wind temperatures (i.e., 280 K, 290 K, 296 K, and 310 K) are simulated to investigate the effect of environmental wind temperature on the cryogenic plume dispersion. In these cases, the other parameters are constant: the environmental wind speed is 1 m/s; the relative humidity is 50%; the exhaust flow rate of the low temperature (110 K) nitrogen gas is 5.6 kg/s.

The simulated minimal oxygen concentration and minimal temperature at H=1.5 m with different environmental wind temperatures are presented in Fig. 8. It is obvious that raising environmental wind temperature has a positive effect on the plume temperature as a large temperature difference enhances the heat exchange and accelerates heating. It is known that a smaller local temperature difference leads to slower descent due to a smaller local density difference. However, the minimal oxygen concentration at H=1.5 m fluctuates, which seems contrary to our ordinary intuition. A reasonable explanation for the result is that the oxygen concentration in the environment drops down as the environmental temperature increases with the constant relative humidity, due to the growing ratio of water vapor in the environmental air. Under the interaction of the two opposite trends, the minimal oxygen concentration at H=1.5 m slightly waves. The fluctuation of the maximum liquid water concentration at H=1.5 m, as shown in Table 5, can also be interpreted on the same basis.

5.3 Effect of relative humidity

Cases with different relative humidity (i.e. 10%, 30%, 50%, 70%, and 90%) are simulated to

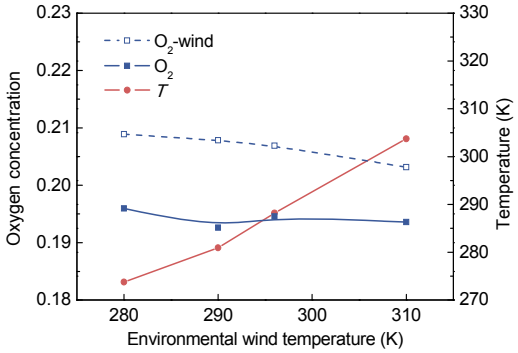

Fig. 8 Simulated minimal oxygen concentrations and minimal temperatures at H=1.5 m with different environmental wind temperatures

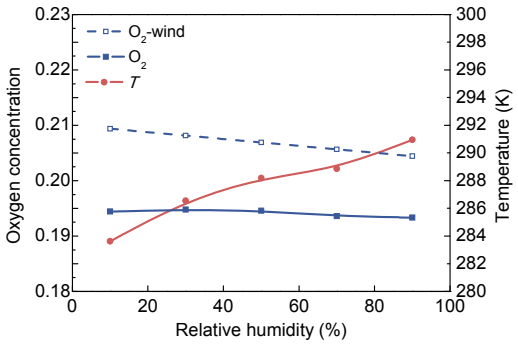

Fig. 9 Simulated minimal oxygen concentrations and minimal temperatures at H=1.5 m with different relative humidity

Table 5 Simulated results of water concentration with different environmental wind temperatures

Environmental wind temperature (K)	Max liquid water concentration in the whole domain (g/m^3)	Max liquid water concentration at H=1.5 m (g/m^3)
280	4.29	3.12
290	8.19	2.97
296	10.42	2.44
310	19.95	3.27

Table 6 Simulated results of water concentration with different relative humidity

Relative humidity (%)	Max liquid water concentration in the whole domain (g/m^3)	Max liquid water concentration at H=1.5 m (g/m^3)
10	2.30	0.86
30	6.97	1.86
50	10.42	2.44
70	15.08	3.50
90	17.04	3.70

investigate the effect of relative humidity on the cryogenic plume dispersion. In these cases, the other parameters are constant: the environmental wind temperature is 296 K; the environmental wind speed is 1 m/s; the exhaust flow rate of the low temperature (110 K) nitrogen gas is 5.6 kg/s.

Fig. 9 depicts the simulated minimal oxygen concentrations and minimal temperatures at H=1.5 m with different relative humidities. As shown in Fig. 9, the relative humidity is a significant influence on the plume temperature near the ground. Higher relative humidity leads more water vapor to interact with the plume gas while the water condensation process will release additional heat exchange between the plume gas and the ambient air. Similar to the content mentioned in Section 5.2, the oxygen concentration in the environment decreases as the relative humidity increases with the constant environmental temperature, since the ratio of water vapor in the environmental air grows. Though the enhanced heat transfer with higher humidity results in a smaller temperature difference, this effect on the oxygen concentration after descent is negligible. As presented in Table 6, the relative humidity has a significant positive impact on the water concentration.

5.4 Effect of exhaust flow rate

The effect of exhaust flow rate on plume dispersion can be divided into two opposite aspects. It is obvious that more nitrogen released per unit time leads to higher nitrogen concentration near the vent stack, which is not conducive to the dissipation of the plume gas. On the other hand, it should be noticed that a higher exhaust flow rate means larger initial kinetic energy. Therefore, more ambient air is entrained in the plume near the vent stack. Meanwhile, the low temperature nitrogen gas will go higher, and thus have a longer distance for descent which is conducive to plume dissipation. Cases with different exhaust flow rates (i.e. 0.06 kg/s, 0.10 kg/s, 0.20 kg/s, 0.50 kg/s, 1.00 kg/s, 2.00 kg/s, 4.00 kg/s, and 5.60 g/s, with an exhaust temperature of 110 K) are simulated to investigate the effect of exhaust flow rate on the dispersion of the cryogenic plume. In these cases, the other parameters are consistent: the environmental wind temperature is 296 K; the environmental wind speed is 1 m/s; the relative humidity is 50%.

As shown in Fig. 10, the minimal oxygen concentration and the minimal temperature at H=1.5 m

first decrease and then increase as the nitrogen exhaust flow rate is increased. These trends result from the interaction of the two opposite effects of the exhaust flow rate on the plume dissipation. At flow rates less than 2 kg/s, the gas accumulation effect from the increasing flow rate dominates, leading to a negative effect on the plume dissipation. When the flow rate is higher than 2 kg/s, the increased flow rate has a positive effect on the plume dissipation, since the larger initial kinetic energy results in a longer distance for descent. As presented in Table 7, the trend of the maximum liquid water concentration at H=1.5 m is similar to those of the minimal oxygen concentration and the minimal temperature at H= 1.5 m, and it also results from the interaction of the two opposite effects. The maximum liquid water concentration in the whole domain monotonically rises with raising flow rate because of the increasing entrained ambient air.

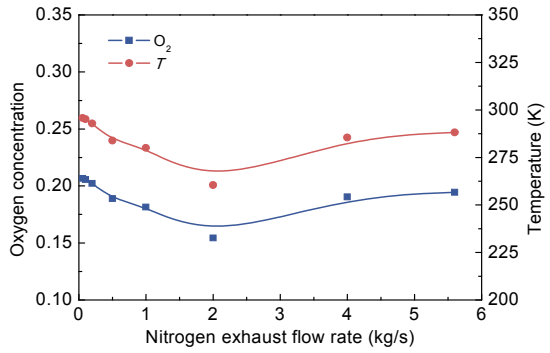

Fig. 10 Simulated minimal oxygen concentrations and minimal temperatures at H=1.5 m with different exhaust flow rates

Table 7 Simulated results of water concentration with different exhaust flow rates

Exhaust flow rate (kg/s)	Max liquid water concentration in the whole domain (g/m^3)	Max liquid water concentration at H=1.5 m (g/m^3)
0.06	5.81	0.06
0.10	7.38	0.34
0.20	7.64	1.02
0.50	8.85	5.47
1.00	8.88	5.89
2.00	9.73	8.34
4.00	9.63	3.08
5.60	10.42	2.44

5.5 Summary of parametric sensitivities of different influence factors

The influences of the environmental wind speed, the environmental wind temperature, the relative humidity, and the exhaust flow rate on the low temperature nitrogen plume dispersion have been simulated and analyzed. In Fig. 11, the effect sensitivities of different influence factors are summarized. The case with the environmental wind speed of 1 m/s, an exhaust flow rate of 5.6 kg/s (@110 K), an environmental wind temperature of 296 K, and a relative humidity of 50%, is set as the reference. The values of the minimal oxygen concentration and the minimal temperature at H=1.5 m for the reference case are both set as 0 in Fig. 11, while the maximum value of the minimal oxygen concentration or the minimal temperature at H=1.5 m with other environmental wind speeds analyzed in this study is set as 1. In other words, the amplitude of variation in the comparison with different environmental wind speeds is set as one reference unit. The amplitude of variation of the minimal oxygen concentration and the minimal temperature at H=1.5 m with the other influence factors are compared with the one with different environmental wind speeds.

In summary, on the temperature of the plume near the ground, the environmental wind temperature and the exhaust flow rate of the nitrogen gas have a greater impact than the environmental wind speed and the relative humidity. On the oxygen concentration near the ground, the exhaust flow rate of the nitrogen gas has greater impact than the environmental wind speed, while the environmental wind temperature and the relative humidity have negligible impacts.

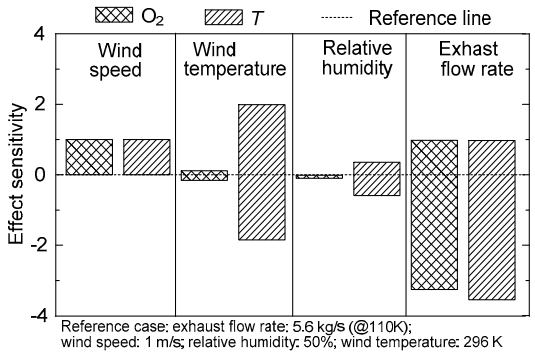

Fig. 11 Effect sensitivities of different influence factors

From the above analyses, the operation of cryogenic wind tunnels should be avoided in harsh weather conditions (i.e. low environmental wind speed, low environmental wind temperature, and high relative humidity). Furthermore, if the weather conditions are unstable and the test is urgent, a low temperature hazard requires attention. If the environmental wind speed fluctuates, prevention of oxygen deficiency should be emphasized. However, variations in the environmental wind temperature and the relative humidity have little impact on oxygen deficiency. Last, but not least, whether prevention of oxygen deficiency and of a low temperature hazard should be taken also depends on the exhaust flow rate of the low temperature nitrogen gas.

6 Conclusions

A numerical model considering the phase change physics of the small quantity of water involved is used to analyze the dispersion of the low temperature nitrogen plume exhausted from a 0.3 m cryogenic wind tunnel. The experiment of the plume exhausting from the US NTF is modeled to validate the numerical model. The CFD calculations with this model are more consistent with the experimental data than those of Lassiter's two-stage analytical model. It can provide acceptable accurate quantitative risk assessments of the cryogenic plume flow behavior to avoid the potential hazards.

Higher environmental wind speeds are conducive to the plume dissipation in respect of oxygen and temperature. Higher environmental wind temperature and relative humidity have a positive impact on plume temperature near the ground, while the oxygen concentration near the ground slightly fluctuates with higher environmental wind temperature and slightly decreases with higher relative humidity. At a flow rate less than 2 kg/s, the gas accumulation effect brought by rising flow rate leads to a negative effect on plume dissipation. When the flow rate is higher than 2 kg/s, increasing flow rates have a positive effect on plume dissipation, since a larger initial kinetic energy results in a longer distance for descent.

The quantitative risk assessment of the cryogenic plume flow behavior is of great significance to avoid potential hazards, and provides a reference for future improvement of the cryogenic gaseous nitrogen discharge systems.

References

ANSYS, 2011. ANSYS FLUENT 14 User's Guide Manual. ANSYS Inc., USA.

Brown TC, Cederwall RT, Chan ST, et al., 1990. Falcon Series Data Report: 1987 LNG Vapor Barrier Verification Field Trials. Technical Report No. UCRL-CR-104316, Lawrence Livermore National Lab, Livermore, CA, USA. https://doi.org/10.2172/6633087

Bruce Jr WE, Fuller D, Igoe WB, 1984. National Transonic Facility shakedown test results and calibration plans. 13th Aerodynamic Testing Conference. https://doi.org/10.2514/6.1984-584

Chan ST, Rodean HC, Ermak DL, 1982. Numerical simulations of atmospheric releases of heavy gases over variable terrain. *In:* de Wispelaere C (Ed.), Air Pollution Modeling and Its Application III. Springer, Boston, MA, USA, p.295-328. https://doi.org/10.1007/978-1-4613-2691-5_20

Ermak DL, Chapman R, Goldwire Jr HC, et al., 1989. Heavy Gas Dispersion Test Summary Report. Technical Report No. ESL-TR-88-22, Lawrence Livermore National Lab, Livermore, CA, USA.

Goldwire Jr HC, Rodean HC, Cederwall RT, et al., 1983. Coyote Series Data Report. LLNL/NWC 1981 LNG Spill Tests Dispersion, Vapor Burn, and Rapid-phase-transition. Vol. 2. Appendices. Technical Report No. UCID-19953-Vol. 2, Lawrence Livermore National Lab, Livermore, CA, USA.

Ivey Jr GW, 1979. Cryogenic gaseous nitrogen discharge system. NASA Conference on Cryogenic Technology, p.271-278.

Kilgore RA, 1976. Design Features and Operational Characteristics of the Langley 0.3-meter Transonic Cryogenic Tunnel. Technical Report No. NASA-TN-D-8304, NASA Langley Research Center, Hampton, VA, USA.

Kilgore RA, 1994. Cryogenic wind tunnels-a brief review. *In:* Kittel P (Ed.), Advances in Cryogenic Engineering. Springer, Boston, MA, USA, p.63-70. https://doi.org/10.1007/978-1-4615-2522-6_7

Kilgore RA, 2005. Evolution and development of cryogenic wind tunnels. 43rd AIAA Aerospace Sciences Meeting and Exhibit. https://doi.org/10.2514/6.2005-457

Koopman RP, Baker J, Cederwall RT, et al., 1982. LLNL/NWC 1980 LNG Spill Tests. Burro Series Data Report: The Appendices. Technical Report No. UCID-19075-Vol. 2, Lawrence Livermore National Lab, Livermore, CA, USA.

Lassiter WS, 1987. Plume Dispersion of the Exhaust from a Cryogenic Wind Tunnel. Technical Report No. NASA-TM-89148, NASA Langley Research Center, Hampton, VA, USA.

Luketa-Hanlin A, Koopman RP, Ermak DL, 2007. On the application of computational fluid dynamics codes for liquefied natural gas dispersion. *Journal of Hazardous Materials*, 140(3):504-517. https://doi.org/10.1016/j.jhazmat.2006.10.023

Marek R, Straub J, 2001. Analysis of the evaporation coefficient and the condensation coefficient of water. *International Journal of Heat and Mass Transfer*, 44(1):39-53. https://doi.org/10.1016/S0017-9310(00)00086-7

McBride MA, Beeves AB, Vanderheyden MD, et al., 2001. Use of advanced techniques to model the dispersion of chlorine in complex terrain. *Process Safety and Environmental Protection*, 79(2):89-102. https://doi.org/10.1205/09575820151095175

Mousavi J, Parvini M, 2016. A sensitivity analysis of parameters affecting the hydrogen release and dispersion using ANOVA method. *International Journal of Hydrogen Energy*, 41(9):5188-5201. https://doi.org/10.1016/j.ijhydene.2016.01.042

NIST (National Institute of Standards and Technology), 2007. NIST Reference Fluid Thermodynamic and Transport Properties Database. NIST, USA.

Ohba R, Kouchi A, Hara T, et al., 2004. Validation of heavy and light gas dispersion models for the safety analysis of LNG tank. *Journal of Loss Prevention in the Process Industries*, 17(5):325-337. https://doi.org/10.1016/j.jlp.2004.06.003

Rubel GO, Gentry JW, 1984. Measurement of the kinetics of solution droplets in the presence of adsorbed monolayers: determination of water accommodation coefficients. *The Journal of Physical Chemistry*, 88(14):3142-3148. https://doi.org/10.1021/j150658a046

Sklavounos S, Rigas F, 2006. Simulation of Coyote series trials—part I: CFD estimation of non-isothermal LNG releases and comparison with box-model predictions. *Chemical Engineering Science*, 61(5):1434-1443. https://doi.org/10.1016/j.ces.2005.08.042

Smelt R, 1945. Power Economy in High Speed Wind Tunnels by Choice of Working Fluid and Temperature. Report No. Aero. 2081, Royal Aircraft Establishment, Farnborough, UK.

Tauseef SM, Rashtchiian D, Abbasi SA, 2011. CFD-based simulation of dense gas dispersion in presence of obstacles. *Journal of Loss Prevention in the Process Industries*, 24(4):371-376. https://doi.org/10.1016/j.jlp.2011.01.014

Zhang XB, Li JF, Zhu JK, et al., 2015. Computational fluid dynamics study on liquefied natural gas dispersion with phase change of water. *International Journal of Heat and Mass Transfer*, 91:347-354. https://doi.org/10.1016/j.ijheatmasstransfer.2015.07.117

中文概要

题　目：基于数值模拟的低温风洞羽流扩散过程的参数敏感性分析

目　的：低温风洞运行时大流量低温氮气被排放到大气环境中，对周围环境造成潜在的低温、缺氧危险。本文旨在研究羽流扩散过程中各变量（环境风速、环境风温度、相对湿度和排气出口流速）对羽流沉降的影响。

创新点：采用考虑相变的低温羽流扩散模型，通过数值模拟对影响羽流扩散的各参数进行敏感性分析。

方　法：1. 基于 Hertz-Knudsen 关系修正，考虑空气中水的相变，构建低温羽流扩散的数值模型；2. 对照美国 National Transonic Facility 的羽流扩散数据和 NASA 的二阶分析模型的计算结果，验证本文所采用的数值模型的准确性；3. 利用数值模拟，比较不同排放条件下近地面的最低氧含量和最低温度，并对各变量进行敏感性分析。

结　论：1. 考虑相变的羽流扩散数值模型，相比 NASA 的二阶分析模型拥有更好的准确性。2. 对于 0.3 m 低温风洞的羽流扩散，高环境风速有利于羽流消散；高环境温度和高相对湿度能提升近地面的最低温度，但对近地面的最低氧含量影响甚微。3. 当排气速度小于 2 kg/s 时，排气流速增大不利于羽流消散；当羽流速度大于 2 kg/s 时，排气流速增大有利于羽流消散。

关键词：低温风洞；羽流扩散；计算流体动力学；相变